ACS APPLIED MATERIALS & INTERFACES

Letter

www.acsami.org

Heterogeneous Solution Deposition of High-Performance Adhesive Hybrid Films

Marta Giachino,[†] Geraud Dubois,*[,†,‡] and Reinhold H. Dauskardt*[,†]

[†]Department of Materials Science and Engineering, Stanford University, Stanford, California 94305, United States

[‡]Hybrid Polymeric Materials, IBM Almaden Research Center, 650 Harry Road, San Jose, California 95120, United States

Supporting Information

ABSTRACT: Interfaces between organic and inorganic materials are of critical importance to the lifetime of devices found in microelectronic chips, organic electronics, photovoltaics, and high-performance laminates. Hybrid organic/inorganic materials synthesized through sol–gel processing are best suited to address these challenges because of the intimate mixing of both components. We demonstrate that deposition from *heterogeneous* sol–gel solutions leads to the unique nanolength-scale control of the through-thickness film composition and therefore the independent optimization of both the bulk and interfacial film properties. Consequently, an outstanding 3-fold improvement in the adhesive/cohesive properties of these hybrid films can be obtained from otherwise identical precursors.

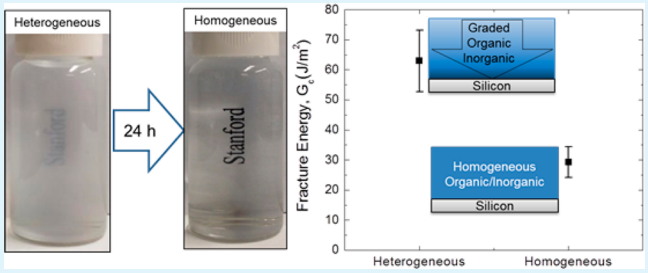

KEYWORDS: *homogeneity, hybrid materials, sol–gel, fracture, thin film*

INTRODUCTION

Liquid-phase deposition has long been carried out from fully homogeneous solutions because of the belief that non-homogeneous solutions can lead to a lack of predictability or reproducibility and poor film properties. We show that deposition from a *heterogeneous* solution presents an innovative strategy to prepare thin films with unique properties that may be unobtainable with classical synthesis routes because of the independent nanolength-scale control of both the *bulk* and *interfacial* properties of these materials. In this study, we focused on a hybrid organic/inorganic system designed to address the bonding of two fundamentally different materials, namely, an organic and an oxide surface, which are found in applications ranging from encapsulation barriers in flexible electronics to multilayer fiber–metal laminates for aerospace applications.[1−8] We found that the full benefit of the hybrid nature of these materials can be achieved when films are deposited from heterogeneous solutions, whereby it becomes possible to control the distribution of the organic and inorganic molecular components throughout the film thickness. As a result, when we introduce this film at the interface between an organic and inorganic material, we can improve the adhesion by up to 3-fold.

Typically, hybrid organic/inorganic materials synthesized through sol–gel processing present superior properties resulting from the nanolength-scale mixing of both components.[9,10] For instance, the system comprised of two primary precursors, an epoxysilane, (3-glycidoxypropyl)trimethoxysilane (GPTMS), and a zirconium alkoxide, tetra-*n*-propoxyzirconium (TPOZ), has been investigated for its ability to bond an oxide surface to an organic material.[11−15] Here, the epoxide group on GPTMS allows chemical cross-linking within the film and guarantees bonding with an adjacent organic layer, while the inorganic silicon/zirconium network binds to an underlying oxide substrate.[11−15] In previous studies, film deposition was always carried out in homogeneous solution conditions.[11−15] As we demonstrate, using a heterogeneous approach allows improved and independent control of the film composition in the bulk and at both interfaces, maximizing the interfacial adhesion and bulk cohesion.

RESULTS AND DISCUSSION

First, we established sol–gel parameters to access both homogeneous and heterogeneous realms of the TPOZ/GPTMS solution. In order to put TPOZ on a similar hydrolysis rate as GPTMS and to prevent fast precipitation of ZrO_2 in water, we reacted TPOZ with acetic acid (TPOZ-Ac) to introduce acetate ligands to the zirconium.[16,17] In addition, we controlled the degree of homogeneity of this system by working in dilute conditions (3.75 wt %) and by varying the sol–gel aging time. This allowed us to obtain a larger window of time to explore the heterogeneous range. Figure 1 shows the transition of the solution from heterogeneous to homogeneous, changing from relatively cloudy but without precipitates to transparent. By controlling this variable, we were able to demonstrate the impact of both the solution state and the deposition parameters, such as the dip-coating speed, on the resulting

Received: July 25, 2013
Accepted: October 2, 2013
Published: October 2, 2013

 © 2013 American Chemical Society

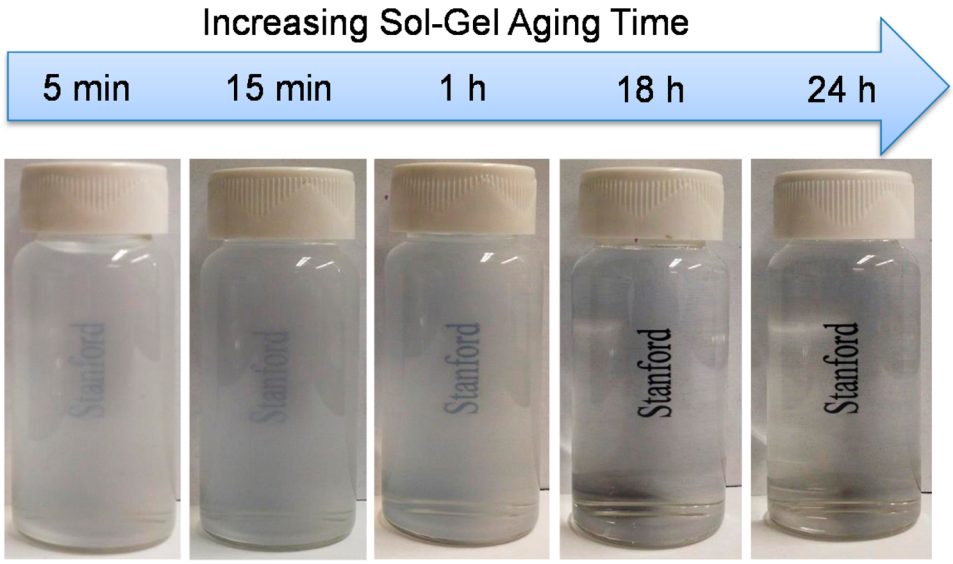

Figure 1. Evolution from heterogeneous to homogeneous of the TPOZ-Ac and GPTMS sol−gel solution in water.

deposited thin-film molecular structure and mechanical properties.

The films were dip-coated with a withdrawal rate of 1 mm s^{-1} from a solution aged for various times with an optimized Zr/GPTMS ratio, which in previous studies has been shown to be approximately 0.7.[12] Using X-ray photoelectron spectroscopy (XPS) depth profiling, we then studied the through-thickness composition of the deposited films. Because of the high carbon (C) content provided by the silane, the C atom percent was used as a trace for the organic network in the film, while the zirconium (Zr) atom percent traced the inorganic network. As shown in Figure 2a, the overall Zr content throughout the films increased with the aging time of the solution, while the total C content of the deposited films decreased systematically with increasing aging time (Figure 2b). This variation in the film composition suggests that the hybrid network deposited on the film varied dramatically from the organic and inorganic contents in solution and was a function of the solution aging time. Furthermore, the XPS data indicated that the Zr and C contents toward the top of the film, i.e., short sputtering time, differed significantly as a function of the aging time. After 1 min of sputtering time (Figure 2a), the Zr content was less than 5 atom % for the 5-min-aged sample, while it increased to more than 10 atom % for the samples aged for 1 h or more. Interestingly, this trend appears to be consistent with a solution transition from heterogeneous to homogeneous that occurs after 1 h of aging (Figure 1). Under the same sputtering conditions, looking at 1 min of sputtering time, the C content decreased with increasing aging time (Figure 2b), contrary to the Zr trend described above. It can be concluded that, by altering the solution homogeneity, we were able to control the organic/inorganic composition throughout the deposited films. As a result, the interfacial adhesive properties of these films to an adjacent organic layer and oxide substrate should also vary significantly with aging time.

The adhesive/cohesive properties of the hybrid layer (HL) were evaluated by measuring the fracture energy, G_c, using a well-established double-cantilever-beam (DCB) test method (see the Experimental Section).[3,6,18] We found that the fracture energy decreased by a factor of 3, from 60 J m^{-2} upon deposition from a heterogeneous solution (5 min of aging

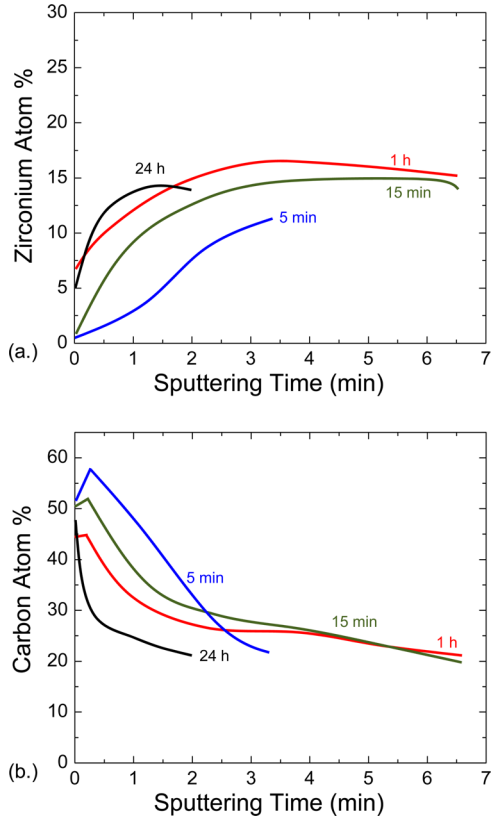

Figure 2. XPS depth profiles of the (a) Zr and (b) C contents in the films deposited from solutions aged for various times. The data indicate the Zr and C contents obtained from sputtering through the film until the HL/silicon interface was reached.

time) to 15 J m^{-2} upon deposition from a homogeneous solution (24 h of aging time; Figure 3). As shown in Figure 3, a decrease in the fracture energy was accompanied by a change in the fracture path. At short aging times, we found that the fracture path meandered through the epoxy film and failed cohesively within the HL, close to the silicon/HL interface. As the aging time increased to 24 h, the fracture path became more uniform and almost completely adhesive between the HL/

dx.doi.org/10.1021/am403032v | ACS Appl. Mater. Interfaces 2013, 5, 9891−9895

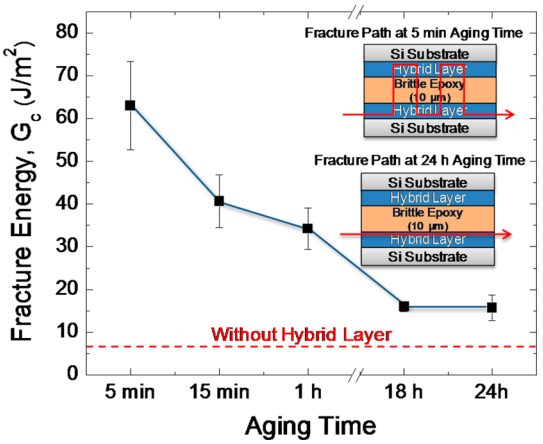

Figure 3. Fracture energy, G_c, of films deposited on silicon substrates as a function of the sol–gel aging time from 5 min to 24 h.

brittle epoxy interface. This shift in the fracture path can be attributed to the change in the organic and inorganic contents of the film and their distribution throughout the film thickness. On the basis of the XPS composition of the films deposited from heterogeneous conditions, the top surface enrichment in organic species led to higher cross-linking at the brittle epoxy/HL interface. The strong bonding of the hybrid film with the adjacent epoxy layer caused the fracture path to force its way through the bonds between the inorganic zirconia network and silicon substrate. For the films deposited from a homogeneous solution, we suggest that the failure path is the result of a lack of organic bonding between the hybrid film and epoxy layer because XPS depth profiling confirmed that these films have lower C content than those deposited from heterogeneous solutions. This demonstrates that the interfacial and bulk network properties of hybrid organic/inorganic films can be separately controlled in a single deposition step. It is evident that this is strongly correlated with the solution state (heterogeneous vs homogeneous), which is a result of the species solubility at a given time and their interaction with the underlying substrate.

We have attempted to correlate the variability in the composition and resulting mechanical properties not only to the hydrolysis and condensation reactions undergone in solution but also to the interaction between the forming network and underlying substrate. It is important to note that the solution opacity emerges when we add TPOZ-Ac to the aqueous GPTMS solution, suggesting that the hydrophobic species are predominantly acetate-bound zirconium and zirconia clusters that are not fully dissolved in water because of their hydrophobicity. This is supported by the fact that zirconium alkoxide precipitates out of solution almost immediately if not stabilized via a coordinating ligand.[16,17,19,20]

Therefore, although stabilization of zirconium slows the hydrolysis/condensation reactions of the compound, it is, nevertheless, fairly insoluble when it is initially added to an aqueous solution but becomes soluble over time as the hydrolysis proceeds. As a result, we suggest that the change in the solubility of the TPOZ-Ac species over time is what induces the transition of the solution from heterogeneous to homogeneous. When the films are deposited via dip coating from a heterogeneous solution, we believe that selective elimination of these hydrophobic species occurs as a result of draining and gravitational forces, resulting in the enrichment of hydrolyzed GPTMS and depletion of the hydrophobic zirconia species. The extent of GPTMS enrichment should also correlate with the degree of hydrolysis and polycondensation of silane in solution. Further studies are currently underway to specifically address this point. Nevertheless, the suggested mechanism above is consistent with our XPS depth profile results for films deposited from a heterogeneous solution, as well as the fracture path results obtained from DCB testing.

Conversely, when the solution is aged for longer times (homogeneous), the zirconia species become more hydrophilic and fully soluble in water. As a result, more zirconium was introduced in the deposited films, which is again consistent with the XPS depth-profiling results described above. Therefore, we expect to see a dependence of the composition and film mechanical properties as a function of the dip-coating speed in heterogeneous systems because the draining forces vary with the withdrawal rates. On the other hand, these should be independent of the deposition conditions at longer aging times.

Next, the substrate dip-coating rate was maintained at 10 mm s^{-1} during film deposition, while the withdrawal rate was varied from 0.2 to 5 mm s^{-1}. For simplicity, we divided the dip-coating withdrawal rates into three categories, namely, slow (0.2 mm s^{-1}), moderate (0.7–1.2 mm s^{-1}), and rapid (3–5 mm s^{-1}). It is worth noting that this overall range (0.2–5 mm s^{-1}) in the dip-coating withdrawal rate corresponds to a well-known "draining regime", whereby the thickness of the film is governed by the equilibrium between the wettability of the solution on the substrate and gravity-induced viscous drag.[21,22] Therefore, a slow withdrawal rate allows time for the solution to recede, leading to thin films, whereas at faster withdrawal rates, there is not enough time for the solution to drain from the substrate, causing thicker films to be deposited.[21] In our experiments, we observed a systematic increase in the thickness of the deposited films with increasing dip-coating withdrawal rates for both the homogeneous and heterogeneous systems, which is consistent with previous dip-coating studies.

We observed a strong dependence of the resulting mechanical properties and film composition on the deposition parameters upon deposition from a heterogeneous solution (Figure 4a), while this dependence was lost for films obtained from a homogeneous solution (Figure 4b). As discussed above, as the solution aged and the precursors evolved to form a homogeneous network, we deposited all of the species in solution, which had become fully soluble. In the homogeneous case, although the films increase in thickness with increasing dip-coating speed, the composition remains the same for all of the films independent of the dip-coating speed (confirmed by XPS depth profiling). This constant composition resulted in a plateau of the fracture energy at ~30 J m^{-2} for all dip-coating rates. These G_c values differ from those obtained during the aging study by ~15 J m^{-2} because of the inherent variability of the sol–gel solutions. By moving to heterogeneous solutions and also utilizing an ideal withdrawal rate, we expect that this draining effect enables selective elimination of hydrophobic species, leaving only those well-anchored to the substrate.

We effectively highlight this selective elimination effect upon deposition from a heterogeneous solution because the fracture energy nearly doubles under optimized dip-coating conditions. At slow dip-coating speeds, i.e., 0.2 mm s^{-1}, we obtained films of about 10–20 nm thickness with poor adhesion, ~30 J m^{-2}. The draining forces in this dip-coating withdrawal rate range are fairly strong, and because the zirconium species are mostly

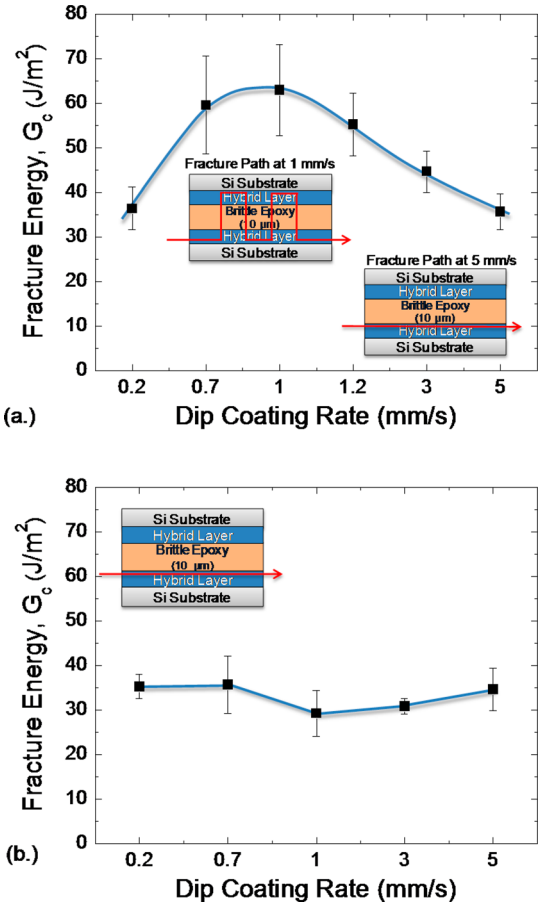

Figure 4. Fracture energy as a function of the dip-coating withdrawal rate for films deposited from (a) a heterogeneous (5-min-aged) solution and (b) a homogeneous (24-h-aged) solution.

hydrophobic under these solution conditions, we obtain very thin films that lack the inorganic network to form a truly hybrid organic/inorganic layer. This very low thickness unfortunately prevented us from clearly identifying the fracture path for these samples. At rapid dip-coating rates, the films were about 120–150 nm thick with fracture energies also of ~30 J m^{-2}. Interestingly, the fracture path here did not match the fracture path previously observed at low aging times but rather resembled that of the 24-h-aged films, i.e., almost entirely adhesive at the HL/epoxy interface. Under these conditions, it is possible that all of the species in solution are deposited, even those that did not fully hydrolyze or condense into a network in solution, leading to nonidealized bonding to the adjacent epoxy. As we moved to moderate withdrawal rates, we obtained films with thicknesses ranging from 60 to 80 nm that incurred a maximum fracture energy of ~60 J m^{-2} at about 1 mm s^{-1}. This suggests that the draining forces in this range are ideal for selectively eliminating only a fraction of the hydrophobic TPOZ-Ac species, while enriching the organic composition, resulting in a molecular structure optimized for strong bonding with both the epoxy and silicon substrate.

CONCLUSION

These results suggest that deposition of thin films in heterogeneous conditions allows us to exploit the multifunctional properties of hybrid systems by gaining full control of the through-thickness composition using a single deposition step. We demonstrate the ability to obtain selective elimination of undesirable species by controlling the solution aging time and dip-coating conditions, resulting in a 3-fold increase in adhesion to an underlying oxide surface and adjacent organic layer. With such nanolength-scale control of the composition and mechanical properties of these films, we envision the synthesis of hybrid materials with targeted properties, such as moisture-resistant adhesion and barrier functionality.

EXPERIMENTAL SECTION

(3-Glycidoxypropyl)trimethoxysilane (GPTMS; Sigma-Aldrich Co., Madison, WI), tetra-*n*-propoxyzirconium (70% in *n*-propyl alcohol, TPOZ; Sigma-Aldrich Co., Madison, WI), and glacial acetic acid (GAA; EMD, Gibbstown, NJ) were used as received. The sol–gel solution consisted of 3.75 wt % solids in solution with a zirconate/GPTMS molar ratio of 0.7. The solution was prepared by first mixing GPTMS with deionized water at 500 rpm at room temperature. In a separate vial, TPOZ (70% in *n*-propyl alcohol) was stabilized with 45 wt % GAA. After the GPTMS/water and TPOZ/GAA solutions were mixed together, the sol was aged from 5 min to 24 h while continuously being stirred at 500 rpm before film deposition. All experimental work was carried out in a laboratory air environment, which remained constant at 25 °C and approximately 40–45% relative humidity. Immediately after the predetermined solution aging time, stirring was stopped and films were deposited by dip coating onto substrates (50 mm × 12.5 mm × 0.777 mm) of a natively oxidized single-crystal [100] silicon. The silicon substrates were submerged in the sol–gel at a rate of 10 mm s^{-1} and immediately withdrawn at rates of 0.2, 0.7, 1, 1.2, 3, and 5 mm s^{-1}. The films were then thermally cured for 2 h at 120 °C in air. The film thickness was measured with a surface profilometer (Dektak 150). X-ray photoelectron spectroscopy (XPS; PHI 5000 Versaprobe system) using an Al Kα X-ray radiation and C60 sputtering was used to measure the through-thickness composition of the as-deposited films.

The fracture energies of the hybrid films were measured in terms of the critical strain energy release rate, G_c, using DCB specimens. The DCB test geometry is a well-established method for measuring the critical strain energy release rates of thin-film structures and interfaces. In this study, DCB test specimens were fabricated by bonding together two sol–gel-coated silicon substrate pieces with a 10-μm-thick bondline of a bisphenol F resin to form a symmetric sandwich test structure. The specimens were then cured at 100 °C for 2 h in air. Subsequently, the DCB specimens were loaded under displacement control at a rate of 0.2 μm s^{-1}, from which a load versus displacement curve was recorded. Equation 1 was used to calculate G_c, whereby P_c is the critical load at which crack growth occurs, a is the crack length, E is the plain strain elastic modulus, and the specimen dimensions are width B and beam thickness h.[23]

$$G_c = \frac{12P_c^2a^2}{B^2E'h^3}\left(1 + 0.64\frac{h}{a}\right)^2 \quad (1)$$

After DCB testing, surface XPS scans along with optical microscopy were used to determine the location of the fracture path in the film stack.

ASSOCIATED CONTENT

Supporting Information

XPS depth profiles of the C and Zr contents in films deposited with 1, 3, and 5 mm s^{-1} dip-coating withdrawal rates from solutions aged for 5 min and 24 h. This material is available free of charge via the Internet at http://pubs.acs.org.

AUTHOR INFORMATION

Corresponding Authors

*E-mail: gdubois@us.ibm.com.
*E-mail: dauskardt@stanford.edu.

Notes

The authors declare no competing financial interest.

■ ACKNOWLEDGMENTS

This research was supported by the Department of Energy (DOE) under Award DEFG0207ER46391.

■ REFERENCES

(1) Dennler, G.; Lungenschmied, C.; Neugebauer, H.; Sariciftci, N. S.; Latreche, M.; Czeremuszkin, G.; Wertheimer, M. R. *Thin Solid Films* **2006**, *511*, 349−353.
(2) Lewis, J. S.; Weaver, M. S. *IEEE J. Sel. Top. Quantum Electron.* **2004**, *10*, 45−57.
(3) Sharratt, B. M.; Wang, L. C.; Dauskardt, R. H. *Acta Mater.* **2007**, *55*, 3601−3609.
(4) Hohlfelder, R. J.; Maidenberg, D. A.; Dauskardt, R. H.; Wei, Y. G.; Hutchinson, J. W. *J. Mater. Res.* **2001**, *16*, 243−255.
(5) Kook, S. Y.; Dauskardt, R. H. *J. Appl. Phys.* **2002**, *91*, 1293−1303.
(6) Snodgrass, J. M.; Pantelidis, D.; Jenkins, M. L.; Bravman, J. C.; Dauskardt, R. H. *Acta Mater.* **2002**, *50*, 2395−2411.
(7) Liu, J.; Chaudhury, M. K.; Berry, D. H.; Seebergh, J. E.; Osborne, J. H.; Blohowiak, K. Y. *J. Adhes. Sci. Technol.* **2006**, *20*, 277−305.
(8) Liu, J.; Chaudhury, M. K.; Berry, D. H.; Seebergh, J. E.; Osborne, J. H.; Blohowiak, K. Y. *J. Adhes.* **2006**, *82*, 487−516.
(9) Mammeri, F.; Le Bourhis, E.; Rozes, L.; Sanchez, C. *J. Mater. Chem.* **2005**, *15*, 3787−3811.
(10) Sanchez, C.; Julian, B.; Belleville, P.; Popall, M. *J. Mater. Chem.* **2005**, *15*, 3559−3592.
(11) Blohowiak, K. Y.; Osborne, J. H.; Krienke, K. A. Sol Coating of Metals. U.S. Patent 5,849,110, Dec 15, 1998.
(12) Oliver, M. S.; Blohowiak, K. Y.; Dauskardt, R. H. *J. Sol−Gel Sci. Technol.* **2010**, *55*, 360−368.
(13) Voevodin, N. N.; Grebasch, N. T.; Soto, W. S.; Kasten, L. S.; Grant, J. T.; Arnold, F. E.; Donley, M. S. *Prog. Org. Coat.* **2001**, *41*, 287−293.
(14) Campazzi, E.; Lancelle-Beltran, E.; Sanchez, C. Particular Nanostructured Material as Protective Coating for Metallic Surfaces. U.S. Patent 0245260 A1, Oct 9, 2008.
(15) Le Blanc, L.; Campazzi, E.; Savigne, P. Sol for Sol−Gel Process Coating of a Surface and Coating Method by Sol-Gel Processing. U.S. Patent 0148711 A1, June 11, 2009.
(16) Yi, G. H.; Sayer, M. *J. Sol−Gel Sci. Technol.* **1996**, *6*, 65−74.
(17) Hayashi, H.; Suzuki, H.; Kaneko, S. *J. Sol−Gel Sci. Technol.* **1998**, *12*, 87−94.
(18) Kook, S. Y.; Snodgrass, J. M.; Kirtikar, A.; Dauskardt, R. H. *J. Electron. Packag.* **1998**, *120*, 328−335.
(19) Doeuff, S.; Henry, M.; Sanchez, C.; Livage, J. *J. Non-Cryst. Solids* **1987**, *89*, 206−216.
(20) Sanchez, C.; Livage, J.; Henry, M.; Babonneau, F. *J. Non-Cryst. Solids* **1988**, *100*, 65−76.
(21) Faustini, M.; Louis, B.; Albouy, P. A.; Kuemmel, M.; Grosso, D. *J. Phys. Chem. C* **2010**, *114*, 7637−7645.
(22) Brinker, C. J.; Frye, G. C.; Hurd, A. J.; Ashley, C. S. *Thin Solid Films* **1991**, *201*, 97−108.
(23) Kanninen, M. F. *Int. J. Fract.* **1973**, *9*, 83−92.